The Impact of a Subpolar North Atlantic Freshwater Anomaly on Eurasian Winter Climate

JEREMY P. GRIST,[a] SIMON A. JOSEY,[a] BABLU SINHA,[a] JAMES A. SCREEN,[b] ROBERT MARSH,[c] AND DIPANJAN DEY[c,d]

[a] *National Oceanography Centre, Southampton, United Kingdom*
[b] *Department of Mathematics and Statistics, Faculty of Environment, Science and Economy, University of Exeter, Exeter, United Kingdom*
[c] *School of Ocean and Earth Science, University of Southampton, Southampton, United Kingdom*
[d] *School of Earth, Ocean and Climate Sciences, Indian Institute of Technology Bhubaneswar, Jatni, Khordha, Odisha, India*

(Manuscript received 29 November 2024, in final form 16 July 2025, accepted 30 July 2025)

ABSTRACT: The potential impact of a subpolar North Atlantic freshwater anomaly on sea surface temperature and the overlying atmosphere on seasonal time scales is investigated. A coupled climate model is perturbed with a major freshwater anomaly (FWA) in the subpolar gyre similar in structure to the 1970s Great Salinity Anomaly (GSA). A 20-member ensemble simulation is run from October to March and compared with a parallel 20-member control simulation. There are robust responses to the FWA in both the ocean and the atmosphere. In the ocean, the FWA is accompanied by an abrupt shoaling of the mixed layer and a decrease in the surface temperature anomalies that stay in place for several months. In the atmosphere, anomalously low pressure develops over the eastern North Atlantic and East Asia. Increased storminess and precipitation develop over the Atlantic (40°–5°W, 30°–55°N) and in the vicinity of Kazakhstan and central Asia (40°–80°E, 35°–50°N). The changes in storminess are consistent with increased horizontal temperature gradients and a stronger and more zonally orientated upper-level jet stream. The ability of the freshwater anomaly to sustain an otherwise short-lived SST anomaly highlights the importance of salinity as an initial condition in coupled seasonal forecasts.

KEYWORDS: Atlantic Ocean; Europe; Atmosphere-ocean interaction; Freshwater

1. Introduction

Recent studies have proposed that a freshwater anomaly in the subpolar North Atlantic could have a significant impact on weather in the Atlantic–European region in subsequent months (Oltmanns et al. 2020, 2024). The proposed mechanism is that anomalous surface freshening in late summer leads to increased ocean surface stratification and a shallower mixed layer. The temperature of a shallower mixed layer is more sensitive to heat loss, resulting in a greater-than-normal SST decrease as seasonal cooling begins. As the freshwater is confined to the subpolar gyre, regions further south do not experience enhanced cooling. Consequently, the winter meridional gradient in SST is increased and this leads to a strengthening of baroclinicity and midlatitude storms.

Hereafter, we refer to Oltmanns' hypothesis as the Salinity to Storminess Mechanism (SSM). We note that there is support for the physical changes associated with the SSM in the literature. For example, the difference between summer and winter subpolar SSTs has increased and is projected to increase further (Chen and Wang 2015; Alexander et al. 2018; Grist et al. 2023), with the change attributed an increase in surface stratification that reduces the volume on which surface fluxes act (Gallego et al. 2018). However, it should be noted that in these studies, increased surface stratification arises primarily from surface warming as opposed to surface freshening. Similarly, it is understood that storms tend to form most frequently and strongly in regions of high baroclinicity (Hoskins and Valdes 1990) and specifically that increases in the midlatitude SST gradient lead to stronger storm tracks (Brayshaw et al. 2008). However, there are some challenges in providing observational evidence for the SSM. First, with global ocean coverage from Argo floats only beginning in the early 2000s, the time period with suitable coverage of sea surface salinity is limited. Second, in a complex coupled system, it is difficult to confidently attribute changes in weather to any one antecedent condition. To this point, while there is recent observational evidence for midlatitude SST anomalies driving an atmospheric response in the North Atlantic Oscillation (e.g., Gastineau and Frankignoul 2015; Wills et al. 2016, 2024), this evidence is mixed and seasonally dependent (see, e.g., Nie et al. 2019).

Considering the current state of understanding of the SSM, in this paper, we isolate the influence of subpolar gyre salinity on the climate system by conducting a 20-member ensemble experiment in which the surface salinity of the subpolar gyre is reduced. The anomaly, though idealized and large, has similarities to the 1970s Great Salinity Anomaly (GSA) (see Dickson et al. 1988). The experiment is conducted with the Hadley Centre Global Environment Model, version 3 (HadGEM3), climate model, a similar version to that used for seasonal forecasts (MacLachlan et al. 2015). The 20-member ensemble control and experiment simulations are run for 6 months starting from 1 October.

The structure of the paper is as follows. The model used, the experimental setup, and the analysis undertaken are described in section 2. In section 3, the results are presented.

Denotes content that is immediately available upon publication as open access.

Corresponding author: Jeremy P. Grist, jeremy.grist@noc.ac.uk

DOI: 10.1175/JCLI-D-24-0669.1

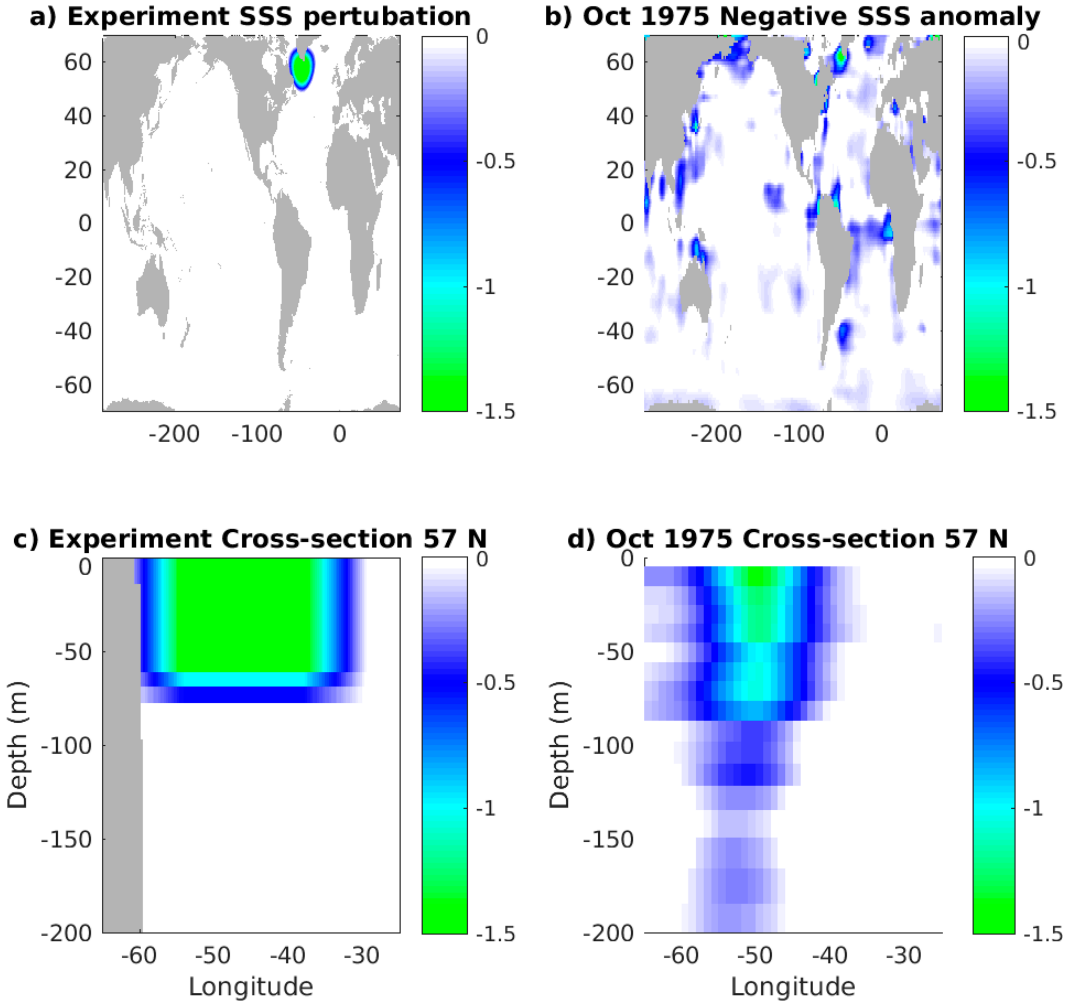

FIG. 1. Difference in 1 Oct salinity initial conditions (psu) between experiment and control simulations (a) surface (SSS) and (c) vertical cross section through the SPG. The observed (EN.4.2.2) anomaly in October 1975 for (b) the surface and (d) a vertical section through the SPG. The anomalies are relative to the 1970–2022 mean.

Finally, in section 4, our results and the implications thereof are summarized.

2. Description of model, experimental setup, and analysis

The model used is the HadGEM3–Global Coupled 3.1 configuration–HM (HadGEM3-GC3.1-MM; Williams et al. 2018; Roberts et al. 2019). It has a ~60-km atmosphere (N216) and an eddy-permitting (~25 km, ¼°) ocean, with 75 levels in the vertical. It has been shown that this resolution is important in minimizing key biases in the ocean and atmosphere and in simulating realistic winter blocking (Scaife et al. 2011). The extent that the representation of blocking frequency patterns is improved by further increasing the resolution of this atmospheric model to 25 km had been examined by Schiemann et al. (2017). Although they found improvements in all seasons, only in March–May was the improvement large compared to the typical distance between ensemble members. The model formed part of the U.K. contribution to CMIP6 (Eyring et al. 2016) and is the basis of that used in the Met Office seasonal prediction system (see Maclachlan et al. 2015; Williams et al. 2018).

With regard to the experimental setup, we note that a control ensemble is initiated from a 10-yr 1950s temperature and salinity climatology (Haarsma et al. 2016). The model is first run from 1 January to 1 October to create 1 October initial conditions. The control ensemble is of 6-month duration from 1 October to 30 March, the following calendar year. The 20 ensemble members were created by changing the initial SST conditions of each grid cell by a random amount between −0.05° and +0.05°C as in Persechino et al. (2013). The experiment followed the same procedure of randomly changing the initial SST field after the initial salinity field had been perturbed. The number of ensemble members is similar to that previously used in HadGEM3 seasonal prediction experiments (Scaife et al. 2014). The perturbation region had a radius of 1000 km centered on the subpolar gyre, specifically 46°N and 57°W (Fig. 1). In the inner part of this region, up to

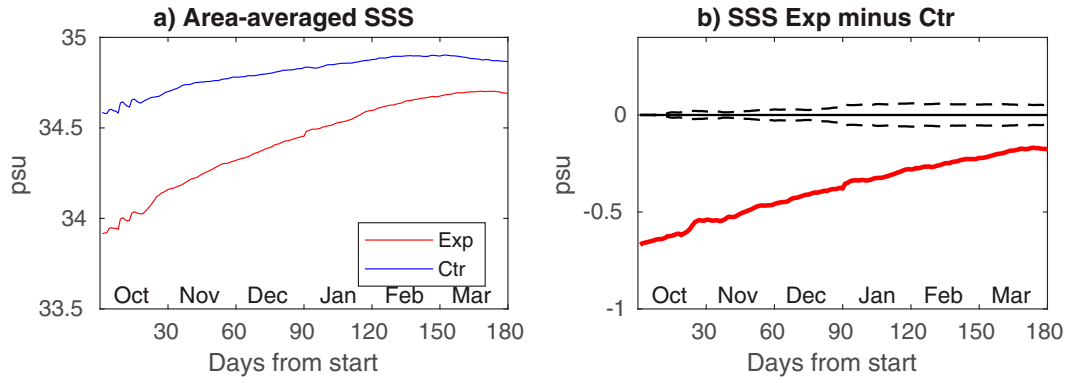

FIG. 2. Daily SSS (psu) area averaged over the SPG perturbation region (Fig. 1a) for (a) the ensemble-mean experiment (red line) and control (blue line). (b) Ensemble-mean experiment minus control (red line). Black dashed lines denote 95% significance.

a radius of 500 km, the salinity is reduced by 1.5 psu, while between 500 and 1000 km, the magnitude of the perturbation is reduced linearly from 1.5 psu to 0. The depth of the perturbation is 54 m with again a linear tapering to 70 m. As a point of reference on 1 October of the control run, the mixed layer depth ranges from 10 to 93 m in the inner region. For additional context, we show from EN4 observations (Good et al. 2013) the salinity anomaly for the GSA period of October 1975 in Figs. 1b and 1b. While this shows the GSA did reach −1.5 psu at the surface, as mentioned, the anomaly was more modest than in the experiment. However, in October 1975, the salinity anomaly of −1.0 psu extended to a width of 600 km wide and reached a maximum depth of 70 m and the −0.5-psu anomaly had a width of about 1000 km and a depth of 90 m.

The experiment design allows significant ocean and atmosphere differences between ensemble-mean experiment and control simulations to be attributed to this freshwater/salinity anomaly in the subpolar gyre (SPG). Similar to the approach used in Grist et al. (2019), ensemble-mean differences are taken to be significant if they exceed the 95th quantile, which for a normal distribution is 1.96 times the standard error. The standard error is defined as the square root of $[(\sigma_p^2/n_p) + (\sigma_c^2/n_c)]$, with σ being the standard deviation of n ensemble members and subscripts p and c referring to the perturbed and control ensembles. To avoid over emphasizing small areas of significance that may be false alarms (Wilks 2006, 2016), a conservative approach to interpretation is adopted and focus is placed mainly on larger, coherent areas of significance.

To track the climate impact of the salinity anomaly, we first examine the ocean salinity, mixed layer depth (MLD), and temperature. We then examine ocean heat loss to the atmosphere and surface atmospheric fields including sea level pressure (SLP), 10-m winds, and 1.5-m air temperature. Following this, changes in upper-level winds are examined and we investigate changes in different measures of storminess (precipitation, vertical motion, and surface storm intensity). For surface storm intensity, we use half the standard deviation of the daily difference in the surface meridional wind as previously used in Booth et al. (2012) and Grist et al. (2021).

3. Results

a. Impact on the ocean

Concentrating first on the changes to the ocean, Fig. 2a shows the experiment and control daily values of the ensemble-mean sea surface salinity (SSS) averaged over the region of the inner part of the freshwater anomaly (FWA) where the 1.5-psu anomaly was applied. The difference in the 2 time series is shown in Fig. 2b. The average anomaly on day 1 is approximately 0.7 psu, and this steadily declines to approximately 0.2 psu by day 180, the end of the 6-month experiment. The persistence of the anomaly is strong enough so that at the end of 6 months, it is still significant. Figure 3 shows how the initial anomaly evolves spatially for each of the 6 months after the start of the experiment. The anomaly largely remains in the initial subpolar gyre regions throughout the 6 months of the experiment. At the 95% level, note there are also isolated, noisy areas of significance elsewhere that are to be expected and are likely a characteristic of the standard significance test used (Wilks 2006, 2016). We note that the spatial extent of the anomaly in the SPG is modulated by the ocean circulation. For example, by month 3, the anomaly has spread south of the Grand Banks, northwest through Davis Strait into Baffin Bay, and northeast through the Irminger Basin toward the Denmark Strait. The extent to which the ocean circulation spreads the anomaly, particularly via the western boundary, is dependent on the ocean resolution, with more energetic eddy-resolving resolutions leading to quicker advection of anomalies (Condron and Winsor 2011, 2012). However, with the experiment duration only being 6 months, we do not expect this to be a critical concern. For example, the typical advection time from the SPG to the tropics greatly exceeds the length of experiment (Weijer et al. 2012).

Robust signals that are geographically distant from the SPG are more likely to be associated with fast ocean teleconnections (Blaker et al. 2006) resulting from the initial disturbance. Additionally, salinity anomalies may arise if the experiment alters the atmosphere in such a way as to modulate the precipitation distribution. For example, we note a small area of negative salinity anomaly that develops near 20°W and 0° in February and March (Figs. 3e,f). The monthly time series of

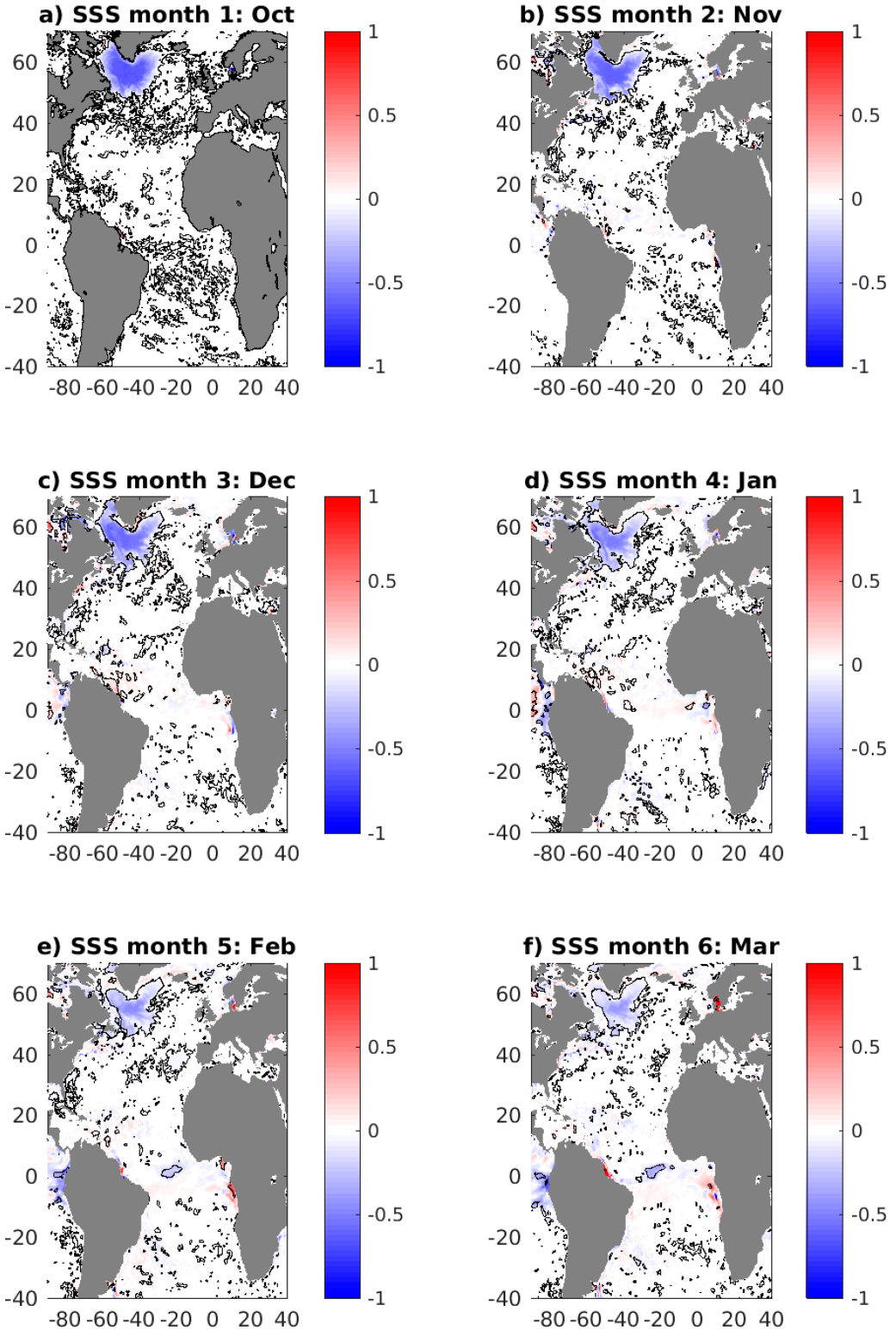

FIG. 3. SSS (psu) ensemble-mean difference between experiment and control simulations for each of the 6 months following the 1 Oct start. Black contours denote 95% significance in the differences. Negative values denote reduced salinity in the experiment.

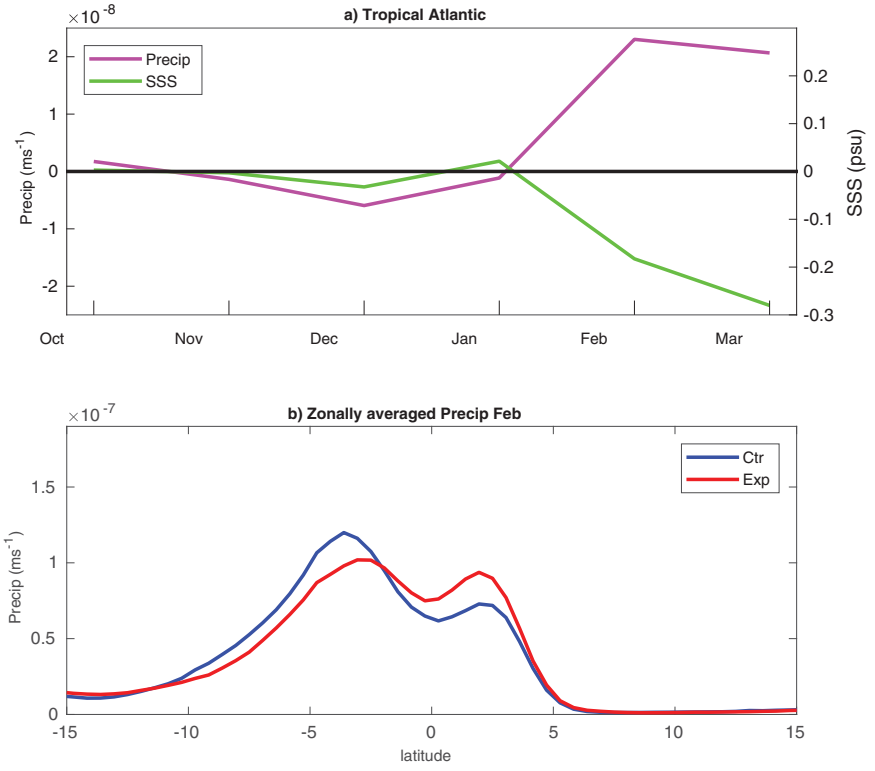

FIG. 4. (a) Ensemble-mean experiment minus control of monthly area-averaged precipitation (m s^{-1}) and SSS (psu) for 27.5°–22°W and 0.5°–2.75°N: precipitation (magenta), SSS (green). (b) Zonally averaged precipitation between 35° and 20°W for the control and experiment ensemble means.

sea surface salinity at this location corresponds well with the precipitation anomaly, suggesting that this particular patch of negative SSS anomaly may be associated with an increase in precipitation (Fig. 4a). The increase in precipitation appears to be associated with a reorganization of the double peak in tropical rainfall associated with the ITCZ (Zhang 2001). Specifically, in the experiment, there is an increase in the northern peak around 0° (Fig. 4b). Salinity anomalies that are both significant and cover a larger area of the tropics would be of interest as a subsequent SST anomaly could have a possible impact on the extratropics. For example, west tropical Pacific SST anomalies can set up an atmospheric Rossby wave train influencing weather systems in North America and in turn the Atlantic Sector (Palmer 2014; Hartmann 2015; Knight et al. 2017). While in general this process is feasible, in this experiment, there is no such wave train from the tropical Pacific in either

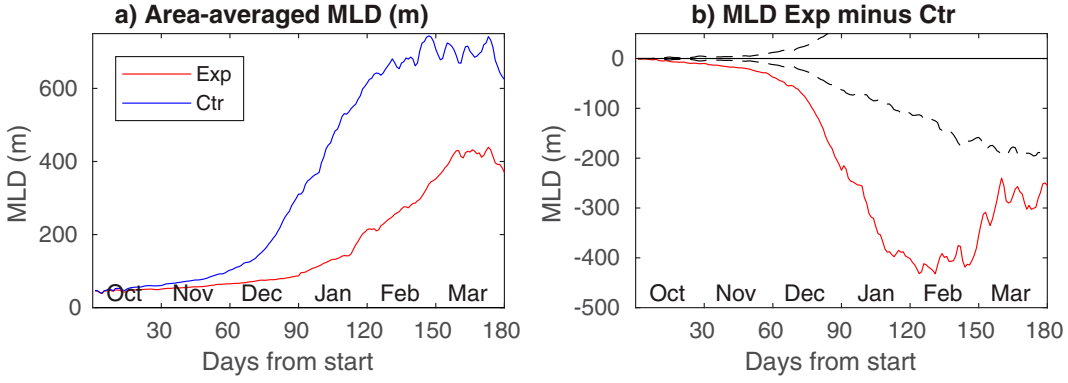

FIG. 5. Daily MLD (m), area averaged over the SPG perturbation region (Fig. 1a) for (a) the ensemble-mean experiment (red line) and control (blue line). (b) Ensemble-mean experiment minus control (red line). Black dashed lines denote 95% significance.

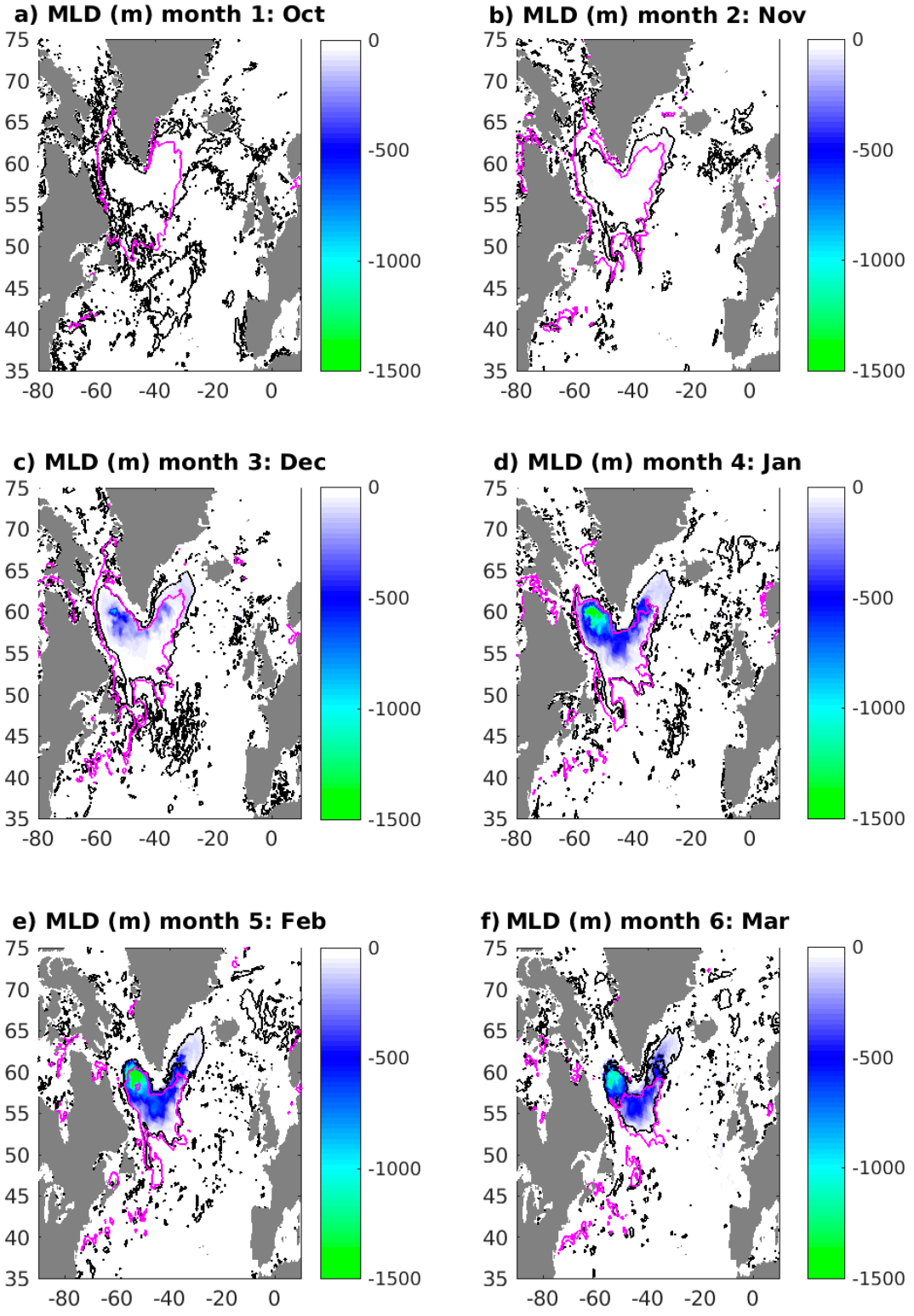

FIG. 6. MLD (m) ensemble-mean difference between experiment and control simulations for each of the 6 months following the 1 Oct start. Black contours denote 95% significance in the differences. Negative values denote shallower mixed layer in the experiment. For reference, the corresponding −0.2 psu contours for the ensemble-mean SSS difference (see Fig. 2) are shown in magenta.

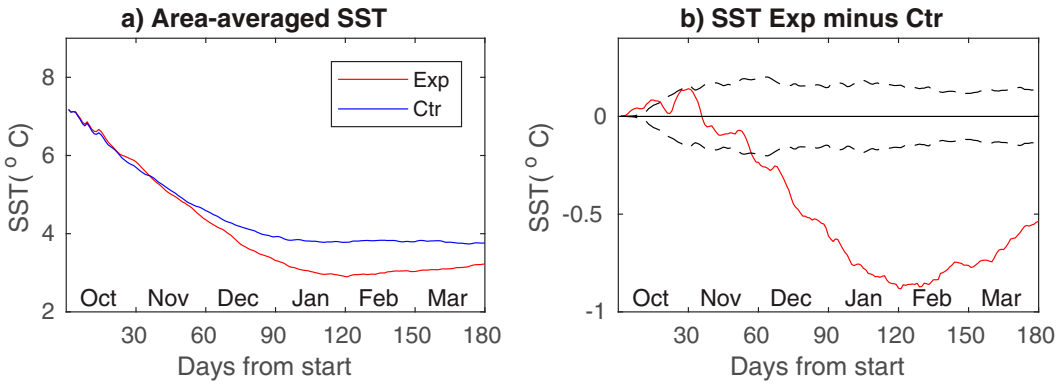

FIG. 7. Daily SST (°C), area averaged over the SPG perturbation region (Fig. 1a) for (a) the ensemble-mean experiment (red line) and control (blue line). (b) Ensemble-mean experiment minus control (red line). Black dashed lines denote 95% significance.

anomalous surface pressure field or the upper-tropospheric geopotential heights. Consequently, the main focus here is considering the direct local and regional impact of the SPG anomaly.

Consistent with the increased stratification brought about by the salinity anomaly, the mixed layer depth shoals in the SPG (Fig. 5a). In October, the MLD is relatively shallow; the area-averaged depth is 53 m for the control, which shoals to 47 m in the experiment. After October, winter heat loss begins to deepen the mixed layer. The mean depth in the control is 78 m in November and then rises rapidly before plateauing near 680 m in February and March. By contrast, the maximum MLD in the experiment is 440 m in March. The effect of the FWA in reducing the MLD increases as the winter mixing increases so that the maximum difference in area-averaged mixed layer is around 405 m near day 125 (February) (Fig. 5b). The evolution of the spatial differences in the mixed layer is shown in Fig. 6. Although significant ensemble differences in the MLD encompass the whole subpolar gyre, there are marked differences within the subpolar gyre. These differences are associated with specific areas, where particularly deep mixing occurs in the control ensemble but is inhibited by stratification in the experiment. For example, differences of over 1500 m in the Labrador Sea reflect the large mixed layer depths (~3000 m) there in January and February of the control ensemble relative to approximately 1500 m in the experiment. It should be noted that, in general, Labrador Sea mixed layer depths are large in the model relative to observations (Koenigk et al. 2021).

Consistent with the shallower mixed layer, a negative SST anomaly develops over the SPG (Fig. 7a). Due to the shallower mixed layer, the surface heat loss to the atmosphere acts on a smaller ocean volume and thus a greater cooling takes place. Figure 7b indicates that the associated difference in temperature becomes significant after about 60 days. The spatial development of the SST anomaly (Fig. 8) reflects that of the SSS anomaly (Fig. 3), apart from a couple of notable modulations. The first of these is a considerable variability of the SST anomaly within the subpolar gyre. In month 4 (January), the western SPG has a much larger SST anomaly than the eastern SPG. To a large extent, such spatial variabilities are consistent with the variability in MLD differences (Fig. 6). The exception to this is later in the experiment, in month 6 (March) where the SST anomaly in the western subpolar gyre begins to fade, despite the continued existence of a large MLD anomaly. The second notable difference is that the SST anomaly clearly extends beyond the region of SSS and MLD anomaly to the south and east. Because this part of the SST anomaly appears to be in the absence of any other oceanographic changes, it may be a consequence of an altered mean atmospheric circulation. Air–sea interaction and the atmospheric responses will be considered more in the next section.

Summarizing the impact on the ocean fields, the FWA results in a shoaling of the mixed layer and a negative temperature anomaly. In this respect, the results are in accord with the expectations of the SSM. However, a notable feature of the anomaly is its persistence. The shoaled mixed layer caused by the FWA remains in place until March (month 6), and as seasonal heat loss continues through this period, so does the negative SST anomaly.

b. Impact on air–sea fluxes and the atmosphere

In this section, we will consider the impact of the FWA on the atmosphere, starting with the net exchange of heat between the ocean and atmosphere. As the SST anomaly becomes significant at around 60 days, we examine the air–sea flux and atmospheric response as the mean of months 3–6. The net heat flux is strongly affected by atmospheric variability, so one might expect less correspondence with the FWA than found in the ocean fields. Nevertheless, all things being equal, one would expect the reduction in SST found in Figs. 7 and 8 to result in less heat loss to the atmosphere. That is to say that once the negative SST anomaly has developed, there will be less heat loss to the atmosphere. Over much of the initial FWA region, this is the case (Fig. 9), although the areas where this is significant are restricted to central and western parts of the initial FWA region. To the south of this is a region of significant negative heat flux anomaly (increased ocean heat loss). This coincides with the region outside the SSS perturbation where there is a negative SST anomaly. The signs of the changes imply that a stronger net heat flux drives the negative SST anomaly, whereas over the FWA region itself, the negative SST anomaly itself leads to a reduction in net heat flux.

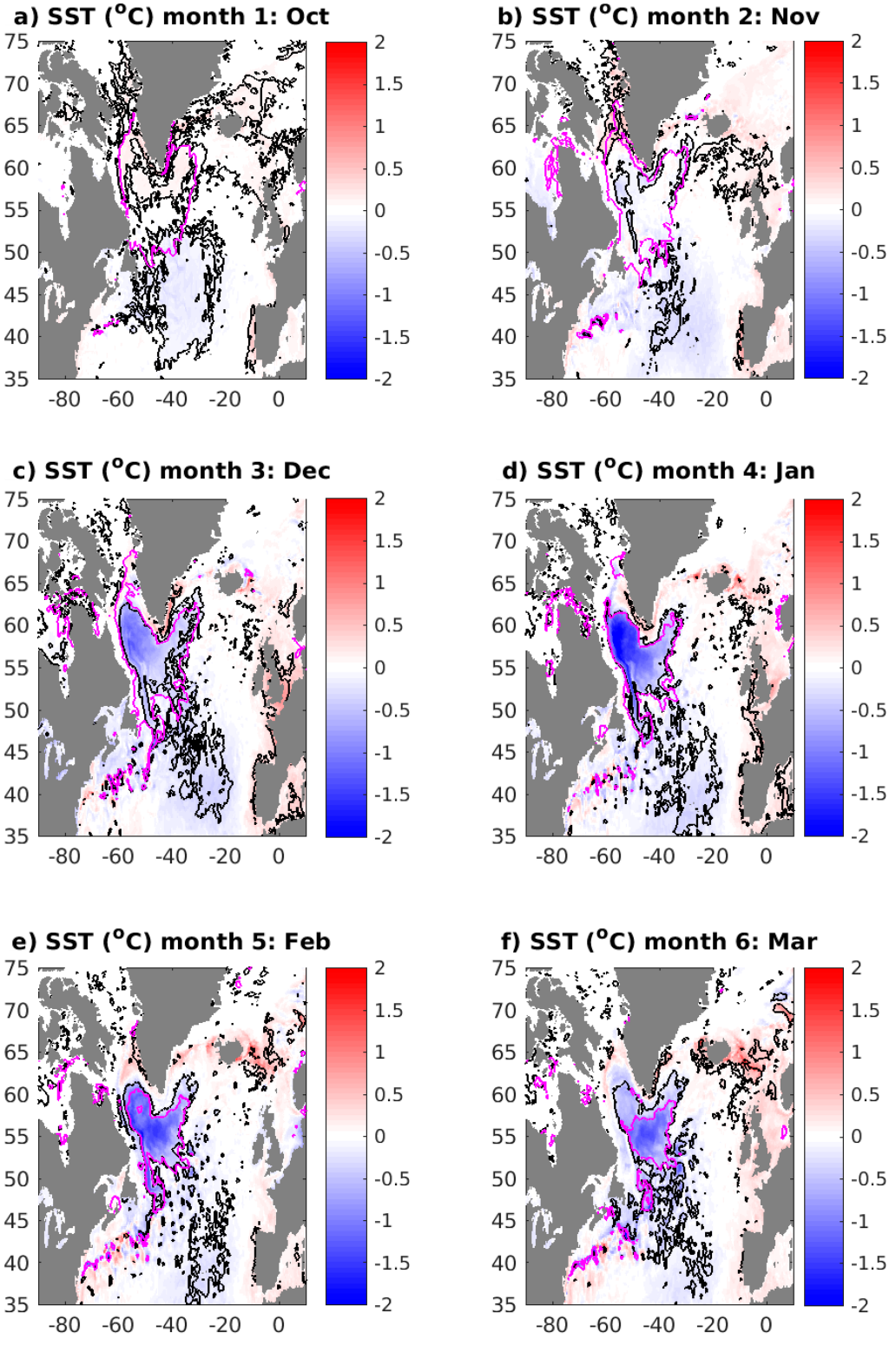

FIG. 8. SST (°C) ensemble-mean difference between experiment and control simulations for each of the 6 months following the 1 Oct start. Black contours denote 95% significance. Negative values indicate colder temperatures in the experiment. For reference, the corresponding −0.2 psu contours for the ensemble-mean SSS difference (see Fig. 2) are shown in magenta.

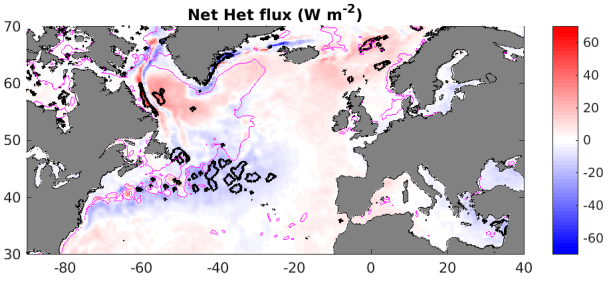

FIG. 9. Net surface air–sea heat flux (W m^{-2}) ensemble-mean difference between experiment and control simulations for the mean of months 3–6 (December–March) following the 1 Oct start. Black contours denote 95% significance. Positive values indicate a reduction in the heat transfer from the ocean to the atmosphere. For reference, the corresponding −0.2 psu contour for the ensemble-mean SSS difference is shown (magenta).

Considering the impact of the FWA on the atmosphere immediately above the ocean surface, the ensemble-mean difference in sea level pressure is shown in Fig. 10a. There is an area of significantly anomalous low pressure just to the east of the FWA, centered on 30°W and 55°N, similar to the east Atlantic pattern (EAP; see, for example, Thornton et al. 2022). This is part of a wave-like disturbance with an anomalously high pressure centered on 20°E and 60°N and another low pressure anomaly centered on 80°E and 60°N. The changes in mean surface winds, shown in Fig. 10a are consistent with the geostrophic changes implied by the anomalous SLP. In conjunction with SLP, we examine the ensemble-mean difference in near-surface (1.5-m) air temperature (Fig. 10b). This field also has a wave-like disturbance, shifted a quarter of a wavelength to the west relative to the pressure pattern. This pattern is expected from anomalous advection resulting from the changes in pressure. We note there are anomalously strong northerlies and westerlies and lower air temperature over the region of negative SST anomalies to the south of the FWA perturbation. This is consistent with the change in the atmosphere forcing in this part of the negative SST anomaly as noted earlier. Directly over the subpolar gyre, however, the negative air temperature anomaly may be associated with less heat being transferred from the ocean to the atmosphere (see Fig. 9). We also note that the negative temperature anomaly is not confined to the surface but manifests in the troposphere, as noted by the negative 1000–700-hPa thickness anomaly (Fig. 10c). The results shown in Fig. 10 indicate not just a thermal response to the atmosphere in the Atlantic basin but a modulation of the mean atmospheric conditions over continental Europe and central Asia, noting particularly the anomalous low surface air temperatures over northwestern Russia, consistent with enhanced northerly advection.

We now consider the extent that surface atmospheric changes are reflected in upper-level geopotential height and zonal wind (Fig. 11). The 500- and 250-hPa geopotential height (Figs. 11a,b) reflect a pattern very similar to the changes in SLP (Fig. 10a), with negative anomalies over mid-Atlantic basin and the central-northern parts of the Ural region and a positive anomaly centered on the Baltic Sea. To the south of each anomaly is an anomaly of the opposite sign in the band 20°–30°N.

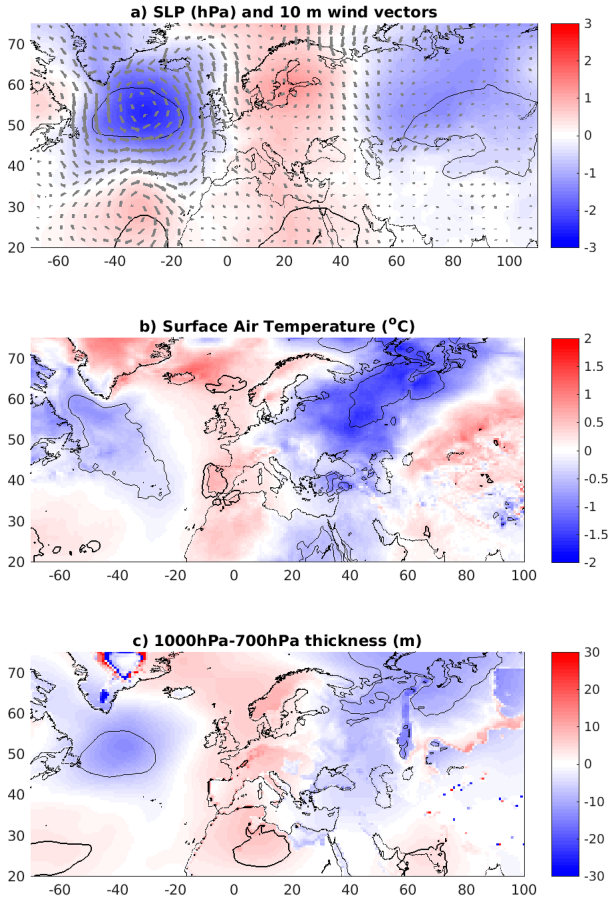

FIG. 10. (a) SLP (shading; hPa) and 10-m wind (vectors) ensemble-mean differences between experiment and control simulations for the mean of months 3–6 (December–March) following the 1 Oct start. (b) As in (a), but for surface (1.5-m) air temperature (°C). (c) As in (a), but for 1000–700-hPa geopotential thickness (m). Black contours denote 95% significance.

The regions where these anomalies are significant are the subpolar and subtropical Atlantic and the Arabian Sea/southern Pakistan. The ensemble-mean differences in 250-hPa zonal wind are shown in Fig. 11c. Over the North Atlantic, there is a band of weakened flow between 55° and 70°N, strengthening immediately to the south. When viewed in conjunction with the ensemble-mean flow (thin green contours in Fig. 11c), it can be seen that this represents the jet stream becoming stronger and more zonal over the North Atlantic. We note again that the atmospheric response over the Atlantic is consistent with the SSM. In addition, the jet is significantly strengthened to the east of the Caspian Sea. It is thus clear that the net effect of the FWA is to modulate the jet stream not only over the Atlantic but also downstream over Eurasia.

We continue examining the atmospheric impact of the FWA in Fig. 12 which shows different measures of storminess and precipitation. There is a significant increase in precipitation in the eastern Atlantic, specifically in the region between 40° and 20°W and 35° and 55°N (Fig. 12a). Consistent with this, similar areas show significant increases in vertical velocity (Fig. 12b)

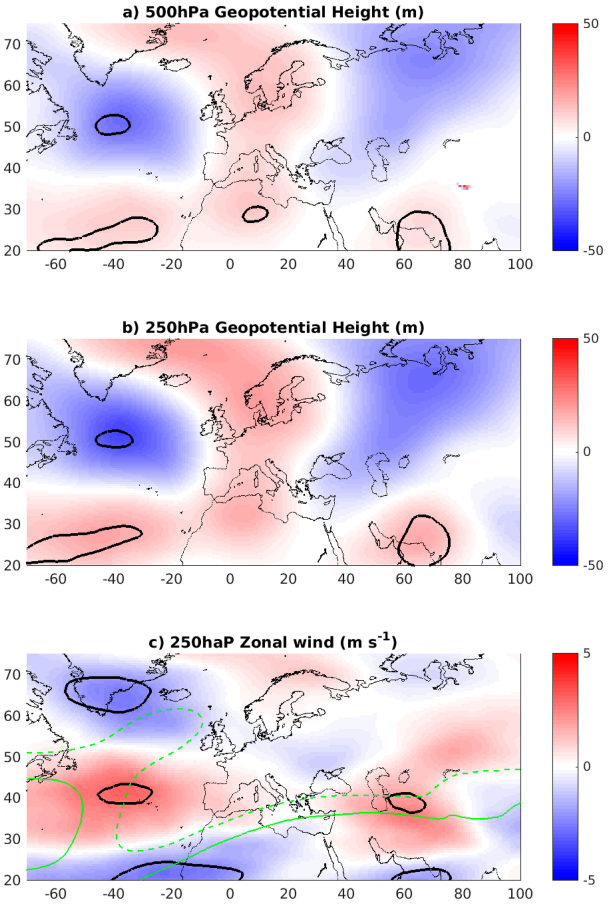

FIG. 11. (a) The 500- and (b) 250-hPa geopotential height (m) ensemble-mean difference between experiment and control simulations for the mean of months 3–6 (December–March) following the 1 Oct start. Black contours denote 95% significance. (c) As in (a) and (b), but for 250-hPa zonal wind (m s^{-1}). Thin green lines in (c) are the 20 and 30 m s^{-1} (dashed) contours of the corresponding 250-hPa mean zonal wind for the same period of the control simulation.

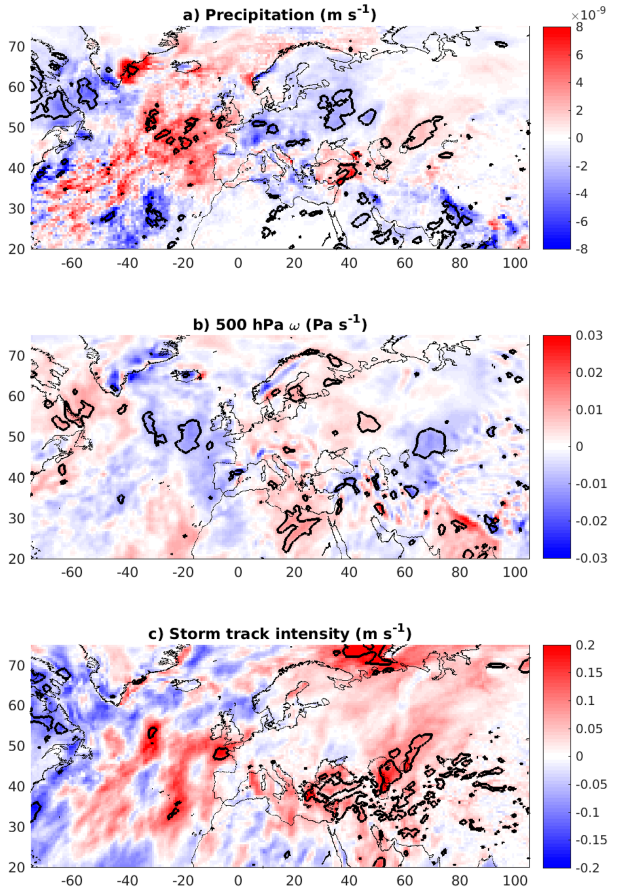

FIG. 12. (a) Precipitation (kg m^{-2} s^{-1}) ensemble-mean differences between experiment and control simulations for the mean of months 3–6 (December–March) following the 1 Oct start. As in (a), but for (b) 500-hPa vertical air motion (i.e., ω; hPa s^{-1}) and (c) surface storm intensity (m s^{-1}). Black contours denote 95% significance.

and surface storm intensity (Fig. 12c). The increase in east Atlantic precipitation in response to the east Atlantic pattern has previously been noted (Josey and Marsh 2005). There is also a response in the region near Kazakhstan (i.e., between 30° and 70°E and 35° and 50°N), which shows significant increases in precipitation, vertical velocity, and storminess. These coherent changes can be interpreted by considering changes to the upper-level flow. In particularly, increases in precipitation and storminess are broadly collocated with the strengthening of the jet stream.

The results in this section have demonstrated that the SST anomaly described in section 3a leads to significant changes from the air–sea interface to the upper troposphere and that these changes influence regional weather systems. More generally, the results here have established that the SSM mechanism can operate in a complex coupled model, and in particular, a freshwater anomaly in the SPG can lead to significant downstream weather impacts on a seasonal time scale.

4. Summary and conclusions

The impact of a North Atlantic SPG freshwater anomaly on both the ocean and the atmosphere has been examined in a coupled climate model experiment. The experiment involved perturbing the initial salinity in a manner that resembled an idealized FWA and the subsequent impact on ocean conditions and the overlying atmosphere on seasonal time scale is investigated. The experiment was motivated by recent studies that proposed that a late summer freshening of the SPG could result in anomalous cooling that impacts storminess by strengthening the meridional SST gradient (Oltmanns et al. 2020). The timing of the study is also pertinent as the North Atlantic is within a period of anomalously low salinity (Holliday et al. 2020) with further freshening projected in coming decades (Marsh et al. 2024).

A 20-member ensemble perturbed simulation run from October to March was compared with a parallel 20-member control simulation. This enabled the impact of a salinity anomaly to be identified in a manner not possible from either observations or long simulations of climate models. In accordance with Oltmanns et al. (2020), the immediate ocean response to the FWA was an abrupt shoaling of the mixed layer

and a decrease in the surface temperature. A notable aspect of the ocean response is that significant salinity and MLD anomalies exist for several months. Consequently, the SST anomaly persists throughout the cooling season.

The strong persistence of the SST anomaly afforded it the opportunity to influence the atmosphere over the following months. The ensemble-mean difference of months 3–6 following the FWA indicates the development of an anomalously low pressure over the eastern North Atlantic and East Asia. Increased storminess and precipitation developed over the Atlantic, east of 40°W, between 30° and 55°N and over central Asia, and between 40°, 80°E and 35°, 50°N. The changes in storminess are consistent with a stronger and more zonal upper-level jet stream.

Although some of the changes such as precipitation increases over the eastern Atlantic are not over human-populated regions, the potential societal impact of the results should not be dismissed. In particular, the severe flooding and storminess in northwest Europe in the winter or 2013–14 were partially associated with an EAP anomaly (Grist et al. 2016; Knight et al. 2017; Thornton et al. 2022), and thus, a slight modulation of the atmospheric response found in this experiment would be of significant societal interest. The observational record does not provide conclusive evidence of a link between the EAP and the North Atlantic sea surface salinity. Although the period of sustained positive EAP index from 2012 to 2017 coincided with an anomalously low salinity in the North Atlantic, during the 1970s GSA, the EAP was predominantly negative (Holliday et al. 2020; Rodrigo 2021). This highlights the challenges in attributing observed changes to any one antecedent condition, which in part motivated the model experiment approach adopted here. However, further sensitivity studies will need to be undertaken to assess the extent the response is dependent on the month in which the FWA appears, as well as its shape and magnitude. It is also reasonable to expect some sensitivity in the results to model resolution. Studies have shown that increases in both atmosphere and ocean resolution enhances the influence of SST on the atmosphere, particularly over the Gulf Stream (Wills et al. 2024, Roberts et al. 2016).

The results here are broadly consistent with the SSM mechanism proposed by Oltmanns et al. (2020). We note that they also propose that fall freshwater anomalies in the SPG are often associated with a negative NAO in the preceding summer and that the net effect of the increased storminess is to increase the NAO index not just in the next winter but also up to the next 3 years. The origin of freshwater anomalies and their potential impact beyond the next winter are of interest but beyond the scope of the current study.

In summary, the experiment confirms that in a complex coupled model, a significant atmospheric impact can arise from a subpolar gyre salinity anomaly. This is broadly consistent with the SSM mechanism proposed by Oltmanns et al. (2020). The atmospheric impacts stretch beyond the Atlantic basin to over central Asia and East Asia and key to this is the FWA's ability to sustain an SST anomaly throughout the cooling season. At a practical level, the results highlight the importance of the accurate representation of salinity fields in the initial conditions of coupled seasonal forecasts.

Acknowledgments. Research was funded by the U.K. Research and Innovation (UKRI) projects ArctiCONNECT (NE/V004875/1) for J. G., S. J., B. S., and J. A. S. and WISHBONE (NE/T01350/1) for B. S. The model experiments were carried out on the ARCHER2 U.K. National Supercomputing Service (http://www.archer2.ac.uk).

Data availability statement. Model experiment data will be made available in the CEDA archive www.ceda.ac.uk.

REFERENCES

Alexander, M. A., J. D. Scott, K. D. Friedland, K. E. Mills, J. A. Nye, A. J. Pershing, and A. C. Thomas, 2018: Projected sea surface temperature over the 21st century: Changes in the mean, variability and extremes for large marine ecosystem regions of northern oceans. *Elementa: Sci. Anthropocene*, **6**, 9, https://doi.org/10.1525/elementa.191.

Blaker, A. T., B. Sinha, V. O. Ivchenko, N. C. Wells, and V. B. Zalesny, 2006: Identifying the roles of the ocean and atmosphere in creating a rapid equatorial response to a Southern Ocean anomaly. *Geophys. Res. Lett.*, **33**, L06720, https://doi.org./10.1029/2005GL025474.

Booth, J. F., L. Thompson, J. Patoux, and K. A. Kelly, 2012: Sensitivity of midlatitude storm intensification to perturbations in the sea surface temperature near the Gulf Stream. *Mon. Wea. Rev.*, **140**, 1241–1256, https://doi.org/10.1175/MWR-D-11-00195.1.

Brayshaw, D. J., B. Hoskins, and M. Blackburn, 2008: The storm-track response to idealized SST perturbations in an aquaplanet GCM. *J. Atmos. Sci.*, **65**, 2842–2860, https://doi.org/10.1175/2008JAS2657.1.

Chen, C., and G. Wang, 2015: Role of North Pacific mixed layer in the response of SST annual cycle to global warming. *J. Climate*, **28**, 9451–9458, https://doi.org/10.1175/JCLI-D-14-00349.1.

Condron, A., and P. Winsor, 2011: A subtropical fate awaited freshwater discharged from Glacial Lake Agassiz. *Geophys. Res. Lett.*, **38**, L03705, https://doi.org/10.1029/2010GL046011.

——, and ——, 2012: Meltwater routing and the Younger Dryas. *Proc. Natl. Acad. Sci. USA*, **109**, 19 928–19 933, https://doi.org/10.1073/pnas.1207381109.

Dickson, R. R., J. Meincke, S.-A. Malmberg, and A. J. Lee, 1988: The "Great Salinity Anomaly" in the northern North Atlantic 1968–1982. *Prog. Oceanogr.*, **20**, 103–151, https://doi.org/10.1016/0079-6611(88)90049-3.

Eyring, V., S. Boniy, G. A. Meehl, C. A. Senior, B. Stevens, R. J. Stouffer, and K. E. Taylor, 2016: Overview of the Coupled Model Intercomparison Project Phase 6 (CMIP6) experimental design and organization. *Geosci. Model Dev.*, **9**, 1937–1958, https://doi.org/10.5194/gmd-9-1937-2016.

Gallego, M. A., A. Timmermann, T. Friedrich, and R. E. Zeebe, 2018: Drivers of future seasonal cycle changes in oceanic pCO_2. *Biogeosciences*, **15**, 5315–5327, https://doi.org/10.5194/bg-15-5315-2018.

Gastineau, G., and C. Frankignoul, 2015: Influence of the North Atlantic SST variability on the atmospheric circulation during the twentieth century. *J. Climate*, **28**, 1396–1416, https://doi.org/10.1175/JCLI-D-14-00424.1.

Good, S. A., M. J. Martin, and N. A. Rayner, 2013: EN4: Quality controlled ocean temperature and salinity profiles and monthly objective analyses with uncertainty estimates. *J. Geophys. Res. Oceans*, **118**, 6704–6716, https://doi.org/10.1002/2013JC009067.

Grist, J. P., S. A. Josey, Z. L. Jacobs, R. Marsh, B. Sinha, and E. Van Sebille, 2016: Extreme air–sea interaction over the North Atlantic subpolar gyre during the winter of 2013–2014

and its sub-surface legacy. *Climate Dyn.*, **46**, 4027–4045, https://doi.org/10.1007/s00382-015-2819-3.

——, and Coauthors, 2019: Re-emergence of North Atlantic subsurface ocean temperature anomalies in a seasonal forecast system. *Climate Dyn.*, **53**, 4799–4820, https://doi.org/10.1007/s00382-019-04826-w.

——, S. A. Josey, B. Sinha, J. L. Catto, M. J. Roberts, and A. C. Coward, 2021: Future evolution of an eddy rich ocean associated with enhanced East Atlantic storminess in a coupled model projection. *Geophys. Res. Lett.*, **48**, e2021GL092719, https://doi.org/10.1029/2021GL092719.

——, ——, and ——, 2023: Observed and projected changes in North Atlantic seasonal temperature reduction and their drivers. *J. Geophys. Res. Oceans*, **128**, e2023JC019837, https://doi.org/10.1029/2023JC019837.

Haarsma, R. J., and Coauthors, 2016: High Resolution Model Intercomparison Project (HighResMIP v1.0) for CMIP6. *Geosci. Model Dev.*, **9**, 4185–4208, https://doi.org/10.5194/gmd-9-4185-2016.

Hartmann, D. L., 2015: Pacific sea surface temperature and the winter of 2014. *Geophys. Res. Lett.*, **42**, 1894–1902, https://doi.org/10.1002/2015GL063083.

Holliday, N. P., and Coauthors, 2020: Ocean circulation causes the largest freshening event for 120 years in eastern subpolar North Atlantic. *Nat. Commun.*, **11**, 585, https://doi.org/10.1038/s41467-020-14474-y.

Hoskins, B. J., and P. J. Valdes, 1990: On the existence of storm-tracks. *J. Atmos. Sci.*, **47**, 1854–1864, https://doi.org/10.1175/1520-0469(1990)047<1854:OTEOST>2.0.CO;2.

Josey, S. A., and R. Marsh, 2005: Surface freshwater flux variability and recent freshening of the North Atlantic in the eastern subpolar gyre. *J. Geophys. Res.*, **110**, C05008, https://doi.org/10.1029/2004JC002521.

Knight, J. R., and Coauthors, 2017: Global meteorological influences on the record UK rainfall of winter 2013–14. *Environ. Res. Lett.*, **12**, 074001, https://doi.org/10.1088/1748-9326/aa693c.

Koenigk, T., and Coauthors, 2021: Deep mixed ocean volume in the Labrador Sea in HighResMIP models. *Climate Dyn.*, **57**, 1895–1918, https://doi.org/10.1007/s00382-021-05785-x.

MacLachlan, C., and Coauthors, 2015: Global Seasonal forecast system version 5 (GloSea5): A high-resolution seasonal forecast system. *Quart. J. Roy. Meteor. Soc.*, **141**, 1072–1084, https://doi.org/10.1002/qj.2396.

Marsh, R., D. Dey, Y.-D. Lenn, and E. M. Roberts, 2024: Shifts from surface density compensation to projected warming, freshening and stronger stratification in the subpolar North Atlantic. *Climate Dyn.*, **62**, 8227–8253, https://doi.org/10.1007/s00382-024-07336-6.

Nie, Y., H.-L. Ren, and Y. Zang, 2019: The role of extratropical air–sea interaction in the autumn subseasonal variability of the North Atlantic Oscillation. *J. Climate*, **32**, 7697–7712, https://doi.org/10.1175/JCLI-D-19-0060.1.

Oltmanns, M., J. Karstensen, G. W. K. Moore, and S. A. Josey, 2020: Rapid cooling and increased storminess triggered by freshwater in the North Atlantic. *Geophys. Res. Lett.*, **47**, e2020GL087207, https://doi.org/10.1029/2020GL087207.

——, N. P. Holliday, J. Screen, D. G. Evans, S. A. Josey, S. Bacon, and B. I. Moat, 2024: European summer weather linked to North Atlantic freshwater anomalies in preceding years. *Wea. Climate Dyn.*, **5**, 109–132, https://doi.org/10.5194/wcd-5-109-2024.

Palmer, T. N., 2014: Record-breaking winters and global climate change. *Science*, **344**, 803–804, https://doi.org/10.1126/science.1255147.

Persechino, A., J. Mignot, D. Swingedouw, S. Labetoulle, and E. Guilyardi, 2013: Decadal predictability of the Atlantic Meridional Overturning Circulation and climate in the IPSL-CM5A-LR model. *Climate Dyn.*, **40**, 2359–2380, https://doi.org/10.1007/s00382-012-1466-1.

Rodrigo, F. S., 2021: Exploring combined influences of seasonal East Atlantic (EA) and North Atlantic Oscillation (NAO) on the temperature-precipitation relationship in the Iberian Peninsula. *Geosciences*, **11**, 211, https://doi.org/10.3390/geosciences11050211.

Roberts, M. J., H. T. Hewitt, P. Hyder, D. Ferreira, S. A. Josey, M. Mizielinski, and A. Shelly, 2016: Impact of ocean resolution on coupled air-sea fluxes and large-scale climate. *Geophys. Res. Lett.*, **43**, 10 430–10 438, https://doi.org/10.1002/2016GL070559.

——, and Coauthors, 2019: Description of the resolution hierarchy of the global coupled HadGEM3-GC3.1 model as used in CMIP6 HighResMIP experiments. *Geosci. Model Dev.*, **12**, 4999–5028, https://doi.org/10.5194/gmd-12-4999-2019.

Scaife, A. A., and Coauthors, 2011: Improved Atlantic winter blocking in a climate model. *Geophys. Res. Lett.*, **38**, L23703, https://doi.org/10.1029/2011GL049573.

——, and Coauthors, 2014: Skillful long-range prediction of European and North American winters. *Geophys. Res. Lett.*, **41**, 2514–2519, https://doi.org/10.1002/2014GL059637.

Schiemann, R., and Coauthors, 2017: The resolution sensitivity of Northern hemisphere blocking in four 25-km atmospheric global circulation models. *J. Climate*, **30**, 337–358, https://doi.org/10.1175/JCLI-D-16-0100.1.

Thornton, H. E., D. M. Smith, A. A. Scaife, and N. J. Dunstone, 2022: Seasonal predictability of the East Atlantic pattern in late autumn and early winter. *Geophys. Res. Lett.*, **50**, e2022GL100712, https://doi.org/10.1029/2022GL100712.

Weijer, W., M. E. Maltrud, M. W. Hecht, H. A. Dijkstra, and M. A. Kliphuis, 2012: Response of the Atlantic Ocean circulation to Greenland Ice Sheet melting in a strongly-eddying ocean model. *Geophys. Res. Lett.*, **39**, L09606, https://doi.org/10.1029/2012GL051611.

Wilks, D. S., 2006: On "field significance" and the false discovery rate. *J. Appl. Meteor. Climatol.*, **45**, 1181–1189, https://doi.org/10.1175/JAM2404.1.

——, 2016: The stippling shows statistically significant grid points. *Bull. Amer. Meteor. Soc.*, **97**, 2263–2273, https://doi.org/10.1175/BAMS-D-15-00267.1.

Williams, K. D., and Coauthors, 2018: The Met Office Global Coupled model 3.0 and 3.1 (GC3.0 and GC3.1) configurations. *J. Adv. Model. Earth Syst.*, **10**, 357–380, https://doi.org/10.1002/2017MS001115.

Wills, R. C. J., A. R. Herrington, I. R. Simpson, and D. S. Battisti, 2024: Resolving weather fronts increases the large-scale circulation response to Gulf Stream SST anomalies in variable-resolution CESM2 simulations. *J. Adv. Model. Earth Syst.*, **16**, e2023MS004123, https://doi.org/10.1029/2023MS004123.

Wills, S. M., D. W. J. Thompson, and L. M. Ciasto, 2016: On the observed relationships between variability in Gulf Stream sea surface temperatures and the atmospheric circulation over the North Atlantic. *J. Climate*, **29**, 3719–3730, https://doi.org/10.1175/JCLI-D-15-0820.1.

Zhang, C., 2001: Double ITCZs. *J. Geophys. Res.*, **106**, 11 785–11 792, https://doi.org/10.1029/2001JD900046.